AUTOPHAGY
2018, VOL. 14, NO. 11, 1991–2006
https://doi.org/10.1080/15548627.2018.1501132

Taylor & Francis
Taylor & Francis Group

RESEARCH PAPER - BASIC SCIENCE

Defective autophagy in vascular smooth muscle cells enhances cell death and atherosclerosis

Yusuke Osonoi[a,b], Tomoya Mita[a,b,c], Kosuke Azuma[a], Kenichi Nakajima[a], Atsushi Masuyama[a], Hiromasa Goto[a], Yuya Nishida[a], Takeshi Miyatsuka[a,c], Yoshio Fujitani[a,d], Masato Koike[e], Masako Mitsumata[f], and Hirotaka Watada[a,b,c]

[a]Department of Metabolism & Endocrinology, Juntendo University Graduate School of Medicine, 2-1-1 Hongo, Bunkyo-ku, Tokyo 113-8421, Japan; [b]Center for Identification of Diabetic Therapeutic Targets, Juntendo University Graduate School of Medicine, 2-1-1 Hongo, Bunkyo-ku, Tokyo 113-8421, Japan; [c]Center for Therapeutic Innovations in Diabetes, Juntendo University Graduate School of Medicine, 2-1-1 Hongo, Bunkyo-ku, Tokyo 113-8421, Japan; [d]Laboratory of Developmental Biology and Metabolism, Institute for Molecular and Cellular Regulation, Gunma University, Maebashi, Japan; [e]Department of Cell Biology and Neuroscience, Juntendo University Graduate School of Medicine, Tokyo, Japan; [f]Division of Cardiology, Department of Medicine, Nihon University School of Medicine, Tokyo, Japan

ABSTRACT

Macroautophagy/autophagy is considered as an evolutionarily conserved cellular catabolic process. In this study, we aimed to elucidate the role of autophagy in vascular smooth muscle cells (SMCs) on atherosclerosis. SMCs cultured from mice with SMC-specific deletion of the essential autophagy gene *atg7* (*Atg7cKO*) showed reduced serum-induced cell growth, increased cell death, and decreased cell proliferation rate. Furthermore, 7-ketocholestrerol enhanced apoptosis and the expression of CCL2 (chemokine [C-C motif] ligand 2) with the activation of TRP53, the mouse ortholog of human and rat TP53, in SMCs from *Atg7cKO* mice. In addition, *Atg7cKO* mice crossed with *Apoe* (apolipoprotein E)-deficient mice (*apoeKO; Atg7cKO:apoeKO*) showed reduced medial cellularity and increased TUNEL-positive cells in the descending aorta at 10 weeks of age. Intriguingly, *Atg7cKO: apoeKO* mice fed a Western diet containing 1.25% cholesterol for 14 weeks showed a reduced survival rate. Autopsy of the mice demonstrated the presence of aortic rupture. Analysis of the descending aorta in *Atg7cKO:apoeKO* mice showed increased plaque area, increased TUNEL-positive area, decreased SMC-positive area, accumulation of macrophages in the media, and adventitia and perivascular tissue, increased CCL2 expression in SMCs in the vascular wall, medial disruption, and aneurysm formation. In conclusion, our data suggest that defective autophagy in SMCs enhances atherosclerotic changes with outward arterial remodeling.

ARTICLE HISTORY
Received 10 October 2016
Revised 17 June 2018
Accepted 10 July 2018

KEYWORDS
Aneurysm; atherosclerosis; autophagy; cell death; senescence; smooth muscle cells

Introduction

Macroautophagy (hereafter autophagy) is a highly evolutionarily conserved dynamic recycling system that is essential for cellular renovation and homeostasis [1]. Autophagy acts to selectively degrade long-lived proteins and remove dysfunctional organelles under basal conditions, as well as to promote cell survival by ensuring metabolic supply via degrading cytoplasmic components in bulk and by eliminating defective or damaged organelles during periods of nutrient deprivation or stress. Defective autophagy has been implicated in various human disease, including neurodegenerative diseases [2], cancers [3], heart failure [4], diabetes mellitus [5], and inflammatory bowel disease [6].

Atherosclerosis is a chronic inflammatory disease that can lead to life-threatening diseases, such as myocardial infarction, stroke, and aortic aneurysm [7]. In particular, myocardial infarction and stroke are triggered at least in part by the rupture of unstable plaques in atherosclerotic lesions, which have a thin fibrous cap comprising cells positive for vascular smooth muscle cell (SMC)-markers, and a thickened intima-media complex with an increased number of cells positive for macrophage markers. Whereas the progression of atherosclerosis involves multiple complex processes, the loss of SMCs plays a substantial role in the progression of vascular diseases. In fact, enhanced rates of SMC death are found in the fibrous cap of human atherosclerotic lesions [8], leading to decreased stability of atherosclerotic plaques [9]. Furthermore, chronic apoptosis of SMCs leads to an increase in the size of atherosclerotic lesions in mice [10]. In addition, increased SMC death and decreased SMC density within the medial layer characterizes human arterial aneurysms [11].

Whereas many disease-associated factors, including oxidative stress, reactive lipids, inflammation, mitogens, and metabolic stressors have been shown to induce autophagy in cultured SMCs [12], previous studies demonstrate that the number of autophagosomes is increased in SMCs of the atherosclerotic lesions of humans and rabbits, as analyzed by transmission electron microscopy (TEM) [13]. These data suggest that this change in autophagic activity may be involved in the pathogenesis of atherosclerosis. Previous studies demonstrate that autophagy induced by reactive lipids, such as 4-hydroxynonenal [14], 7-ketocholesterol [15], and excess free cholesterol [16] in SMCs attenuates cell death. In addition, a recent study demonstrates that mice deficient

CONTACT Tomoya Mita tom-m@juntendo.ac.jp Department of Metabolism & Endocrinology, Juntendo University Graduate School of Medicine, 2-1-1 Hongo, Bunkyo-ku, Tokyo 113-8421, Japan
Supplementary data for this article can be accessed here.

specifically in SMC autophagy have enhanced vascular contractility, possibly through the dysregulation of calcium homeostasis in SMCs [17]. Furthermore, mice deficient in autophagy specifically in SMCs show accelerated cell senescence, enhanced neointimal formation after ligation-induced injury, and enhanced atherosclerosis when crossed with *Apoe* (apolipoprotein E)-deficient mice (*apoeKO*) and fed a western-type diet [18]. These data hence demonstrate the protective role of autophagy in SMCs for the progression of atherosclerosis. In this study, we further investigated the role of autophagy in SMCs on the progression of atherosclerosis and identified the unexpected role of SMC autophagy in preventing aortic aneurysm formation *in vivo*.

Results

Autophagy deficiency results in increased susceptibility of SMCs to cell death

To investigate the functional roles of autophagy in SMCs, we used a model with defective autophagy in SMCs. For this purpose, we generated mice with a tissue-specific deletion of *Atg7*, an essential gene for autophagy, in SMCs by crossing $Atg7^{f/f}$ mice with *Tagln* (*transgelin*)/*Sm22αCre*$^{+/0}$ mice (*Atg7cKO*). It is of note that *Tagln* $Cre^{+/0}$ mice are widely used to assess the function of vascular SMCs *in vivo* as TAGLN is expressed in all SMCs, including vascular SMCs [19]. Then, we isolated primary SMCs from *Atg7cKO* mice, as well as $Atg7^{f/f}$ mice as a floxed control. SMCs isolated from *Atg7cKO* mice showed reduced expression of ATG7, and reduced levels of MAP1LC3B (microtubule-associated protein 1 light chain 3 beta)-II, which is a marker of autophagosomes [20], together with the accumulation of SQSTM1 (sequestosome 1), a receptor protein that is degraded by autophagosomes (Figure 1(A)). In SMCs from control $Atg7^{f/f}$ mice, TEM demonstrated normal-shaped mitochondria and a small number of autophagic vacuoles (Figure 1(B)). Compared with the ultrastructure of SMC mitochondria of control $Atg7^{f/f}$ mice, that of *Atg7cKO* mice were heterogenous; some were low in electron density and lacked cristae, whereas some were high in electron density (Figure 1(B)). Furthermore, autophagic vacuoles containing mitochondria were occasionally found in the SMCs of control $Atg7^{f/f}$ mice, whereas autophagic vacuoles were not observed within the SMCs of *Atg7cKO* mice (Figure 1(A,B)). These data suggest that SMCs from *Atg7cKO* mice show defects in autophagy, which play important roles in the removal of dysfunctional organelles.

To investigate the effect of autophagy on cell growth, we counted the number of SMCs during their culture with serum. As shown in Figure 1(C), the number of SMCs from *Atg7cKO* mice, 8 days after the start of culture was significantly lower than that of control $Atg7^{f/f}$ mice. To calculate the cell death ratio during culture, we measured nucleosomes in cytosolic cell lysates. Relative nucleosome concentration of SMCs from *Atg7cKO* was numerically higher after 24 h of culture and significantly higher after 48 h of culture than the control $Atg7^{f/f}$ mice (Figure 1(D)). Along with increased cell death, SMCs from *Atg7cKO* mice demonstrated higher expression of phosphorylated form of H2AFX (H2A histone family member X), a DNA damage marker, than the control $Atg7^{f/f}$ mice (Figure 1(E)). In addition, phosphorylation of TRP53 and BBC3 (BCL2 binding component 3), which is a critical mediator of apoptosis, were significantly increased in SMCs from *Atg7cKO*. As TRP53 is an important regulator of cell senescence, we next performed senescence-associated GLB1 (galactosidase, beta 1) staining. Similar to a previous study [18], *Atg7cKO* mice demonstrated stronger senescence-associated GLB1 staining than that of control $Atg7^{f/f}$ mice (Figure 1(F)). Furthermore, SMCs from *Atg7cKO* mice showed decreased proliferation capacity evaluated by the bromodeoxyuridine (BrdU) incorporation assay (Figure 1(G)).

Oxidative stress is involved in the pathogenesis of atherosclerosis, restenosis [21], and aneurysm formation [22], and was reported to induce SMC death [23]. To investigate the effect of oxidative stress on cell death in SMCs from *Atg7cKO* mice, we analyzed cell numbers after the addition of 100 μM H_2O_2 for 48 h. Similar to a previous study [18], SMCs from *Atg7cKO* mice were more resistant to exogenous high oxidative stress-induced cell death compared with control $Atg7^{f/f}$ mice (Figure 1(H)). Next, we investigated the effect of the antioxidant N-acetylcysteine (NAC) on cytosolic nucleosome levels. Intriguingly, NAC treatment drastically reduced cytosolic nucleosome levels in both SMCs from *Atg7cKO* and control $Atg7^{f/f}$ mice, and its effect appeared to be stronger in *Atg7cKO* mice (Figure 1(I)). Along with the reduction in cell death, NAC treatment significantly suppressed the expression of H2AFX, phosphorylated TRP53, and BBC3 in *Atg7cKO* mice (Figure 1(E)). Although SMCs from *Atg7cKO* mice were much more resistant to exogenous high oxidative stress-induced cell death, cell death of SMCs induced by a defect in autophagy may be mediated at least in part by basal levels of oxidative stress.

Autophagy deficiency in SMCs increases cell death at an early stage of atherosclerosis

To investigate the role of autophagy in SMCs in our atherosclerosis model, we first analyzed the morphology of the descending aorta in *Atg7cKO* mice and control $Atg7^{f/f}$ mice. When *Atg7cKO* mice and control $Atg7^{f/f}$ mice were fed a normal chow diet for 24 weeks, no atherosclerotic lesions were found in both mice (data not shown). Thus, we next crossed *Atg7cKO* mice with *apoeKO* (*Atg7cKO:apoeKO*). At 10 weeks of age, atheromas were not found in both groups (Figure 2(A)). Whereas no SQSTM1-positive cells were observed in cells in the media of the aorta from floxed control $Atg7^{f/f}$*:apoeKO* mice, most cells in the media of the aorta of *Atg7cKO: apoeKO* mice were SQSTM1-positive (Figure 2(B)).

Next, we searched for apoptotic cells by TUNEL assay. Whereas TUNEL-positive cells were hardly observed in the media of control $Atg7^{f/f}$*:apoeKO* mice aortas, we frequently found TUNEL-positive cells in the media of aortas from *Atg7cKO:apoeKO* mice (Figure 2(C)). Probably reflecting this observation, the medial density of SMCs of both thoracic and abdominal aortas from *Atg7cKO:apoeKO* mice analyzed by hematoxylin and eosin staining (Figure 2(D)) and ACTA2 (actin, alpha 2, smooth muscle, aorta) staining (Figure S1) were reduced. Conversely, the number of proliferating cells in

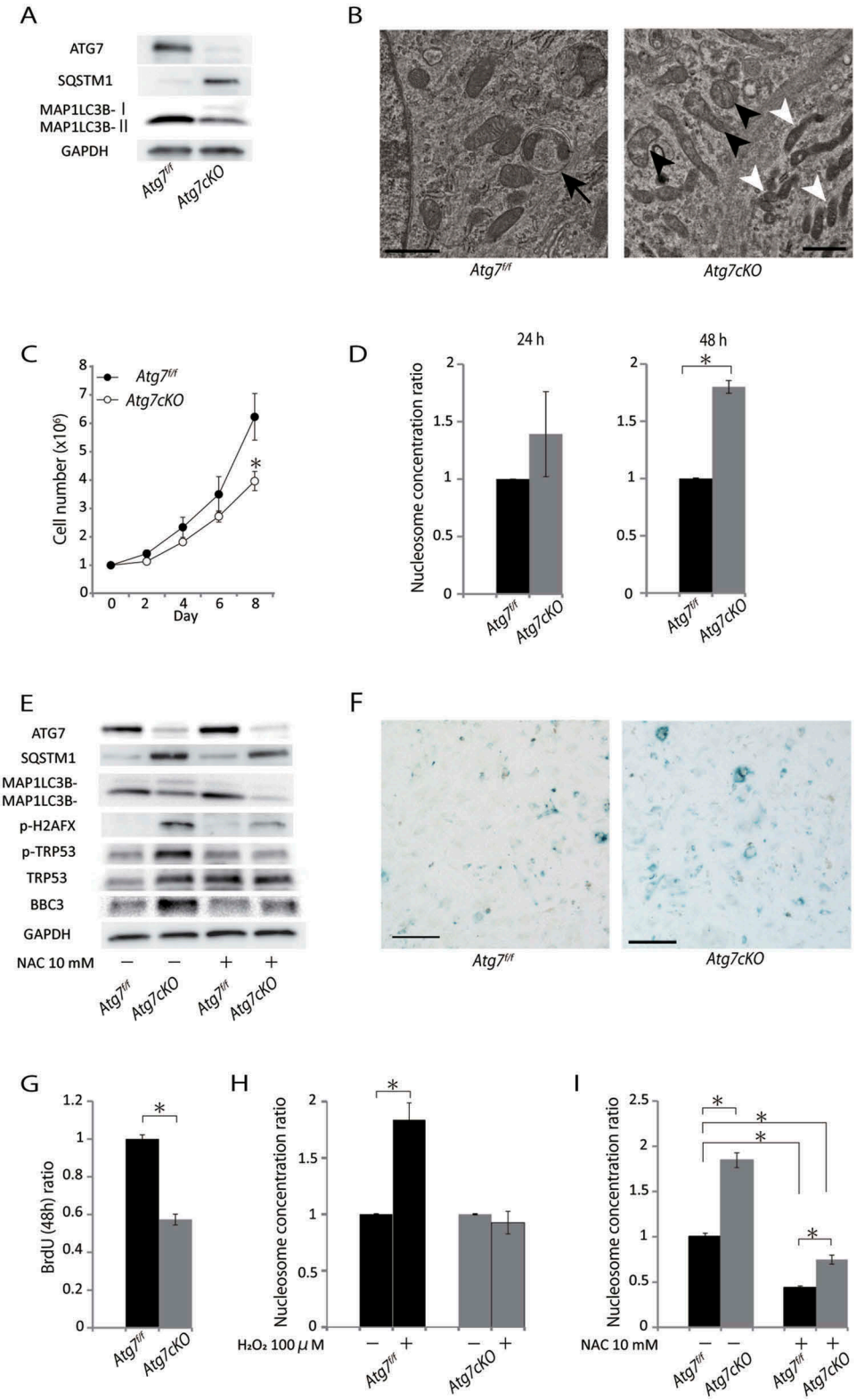

Figure 1. Autophagy deficiency in SMCs increases cell death. SMCs from control *Atg7*$^{f/f}$ and *Atg7cKO* mice at 10 weeks of age were isolated. (A) Western blot analysis of primary isolated SMCs for ATG7, MAP1LC3B-I, MAP1LC3B-II, and SQSTM1. Representative results from 3 independent experiments are shown. (B) TEM of primary isolated SMCs. The black arrow indicates an autophagosome. The black arrowheads indicate ultrastructure of mitochondria lacking cristae with low electron density. The white arrowhead indicates the ultrastructure of mitochondrion with high electron density. Scale bars: 1 μm. (C) Numbers of cultured cells. Data are the mean ± SEM of 5 independent experiments. *$P < 0.05$ vs control *Atg7*$^{f/f}$ mice. (D) Relative nucleosome concentration in SMCs after culturing for 24 h or 48 h. Data are shown as the mean ± SEM of 3 independent experiments. *$P < 0.05$ vs control *Atg7*$^{f/f}$ mice. The data from control SMCs was set to 1.0. (E) Western blot analysis of primary SMCs pretreated with or without N-acetylcysteine (NAC). Representative results from 3 independent experiments are shown. (F) Senescence-associated GLB1 staining of SMCs. Scale bars: 300 μm. (G) Relative BrdU uptake in SMCs. Data are shown as the mean ± SEM of 3 independent experiments. *$P < 0.05$ vs control *Atg7*$^{f/f}$ mice. Data from control SMCs was set to 1.0. (H) Relative increase in nucleosome concentration in SMCs treated with 100 μM H_2O_2 for 48 h. Data are shown as the mean ± SEM of 5 independent experiments. *$P < 0.05$ vs control *Atg7*$^{f/f}$ mice. The data from the control *Atg7*$^{f/f}$ and *Atg7cKO* without 100 μM H_2O_2 was set to 1.0 respectively. (I) Relative nucleosome concentration in SMCs pretreated with or without NAC for 48 h. Data are shown as the mean ± SEM of 3 independent experiments. *$P < 0.05$ vs control *Atg7*$^{f/f}$ mice. The data from the control SMCs was set to 1.0.

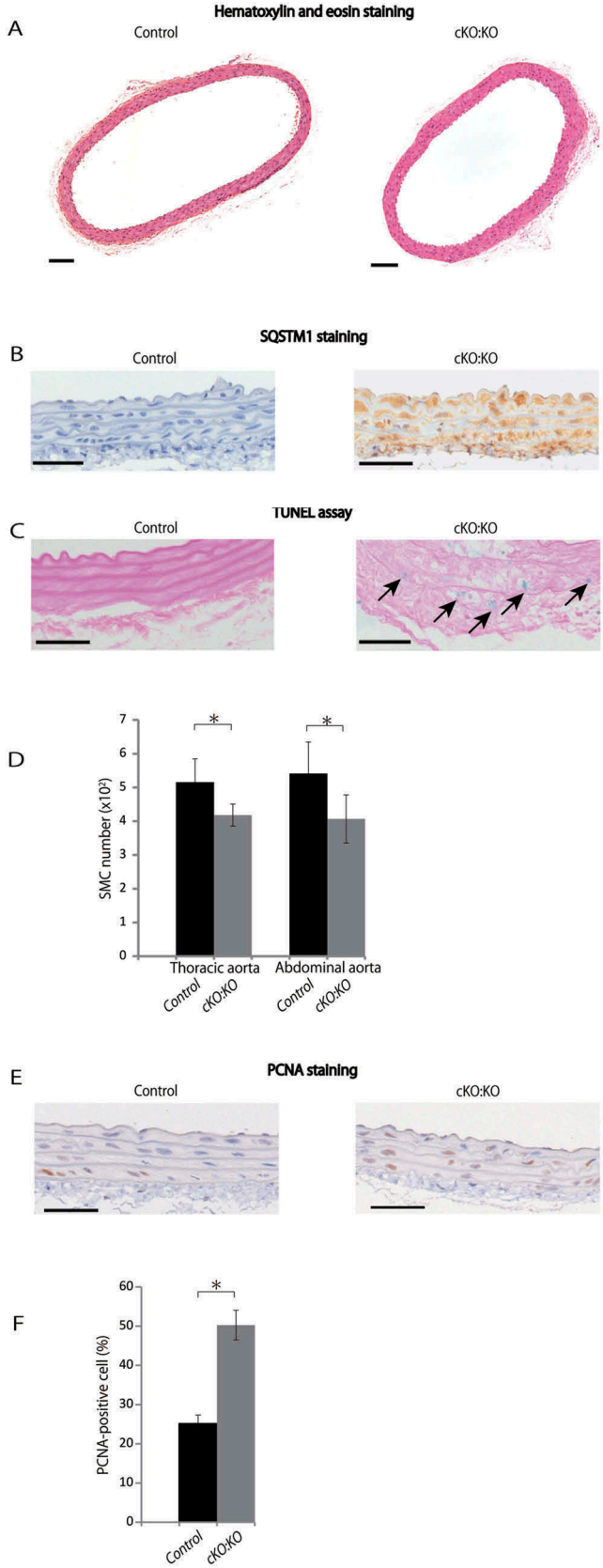

Figure 2. Autophagy deficiency in SMCs reduces medial cellularity. Sections of descending aortas from control *Atg7*$^{f/f}$*:apoeKO* mice (Control) and *Atg7cKO:apoeKO* mice (cKO:KO) at 10 weeks of age were evaluated. (A) Representative histological sections of descending aortas stained with hematoxylin and eosin. Scale bars: 100 µm. (B) Representative histological sections of descending aortas stained with a SQSTM1 antibody and hematoxylin. Scale bars: 50 µm. (C) Representative photographs of sections of the descending aorta subjected to the TUNEL assay and stained with Red Counterstain C. Arrows indicate TUNEL-positive cells. Scale bars: 50 µm. (D) Medial SMC numbers were evaluated in the thoracic aorta and abdominal aorta by hematoxylin and eosin staining. Data are shown the mean ± SEM of 11. *$P < 0.05$ vs Control. (E) Representative histological sections of descending aortas stained with antibodies against PCNA (proliferating cell nuclear antigen) and with hematoxylin. Scale bars: 50 µm. (F) PCNA-positive cell numbers were analyzed in the descending aorta. Data are shown as the mean ± SEM of 11 samples. *$P < 0.05$ vs Control.

the media of *Atg7cKO:apoeKO* mice aortas evaluated by proliferating cell nuclear antigen (PCNA) were increased compared with control *Atg7$^{f/f}$:apoeKO* mice, probably due to a compensation mechanism [24] (Figure 2(E,F)).

Atg7cKO:apoeKO mice fed a Western diet showed increased premature death

Control *Atg7$^{f/f}$:apoeKO* mice and *Atg7cKO:apoeKO* mice fed a normal chow diet for 24 weeks did not show any differences in their survival rates (Figure 3(A)). Thus, to further investigate the roles of SMC autophagy in atherosclerosis, control *Atg7$^{f/f}$:apoeKO* mice and *Atg7cKO:apoeKO* mice at the age of 10 weeks were fed a Western diet for 14 weeks. After a 14-week Western-diet load, body weight and food consumption of *Atg7cKO:apoeKO* mice were slightly decreased compared with control *Atg7$^{f/f}$:apoeKO* mice (Table 1). In addition, *Atg7cKO:apoeKO* mice showed modest but significantly decreased levels of total cholesterol, high-density lipoprotein-cholesterol, and triglyceride (Table 1). These differences in lipid parameters may be associated with the small reduction in food consumption of *Atg7cKO:apoeKO* mice. Conversely, there was no significant difference in mean systemic arterial pressure between the 2 groups (Table 1). Intriguingly, Kaplan-Meier curves showed that the survival rates of *Atg7cKO:apoeKO* mice were significantly reduced compared with control *Atg7$^{f/f}$:apoeKO* mice (Figure 3(B)). Autopsy of some of the dead mice showed the coagulation of blood in the thoracic or abdominal cavity and cracks in the aorta, suggesting that these mice died of aortic rupture (Figure 3(C)).

Next, we analyzed the whole aorta by oil-red O staining, as a marker of atherosclerotic area in *Atg7cKO:apoeKO* mice and control *Atg7$^{f/f}$:apoeKO* mice fed a Western diet. As shown in Figure 4(A,B), the area stained with oil-red O in *Atg7cKO:apoeKO* mice was larger than control *Atg7$^{f/f}$:apoeKO* mice fed a Western diet. In addition, we measured maximum diameters of the suprarenal abdominal aorta, which is generally regarded as the main site of aneurysm formation [25]. Although the maximal external diameter of the suprarenal aorta was similar between control *Atg7$^{f/f}$:apoeKO* mice and *Atg7cKO:apoeKO* mice fed a normal chow diet, it was significantly larger in *Atg7cKO:apoeKO* mice than in the control *Atg7$^{f/f}$:apoeKO* mice under Western diet (Figure 4(C,D)), supporting the idea that autophagy deficiency in SMCs induces the progression of atherosclerosis and a higher frequency of aneurysm formation.

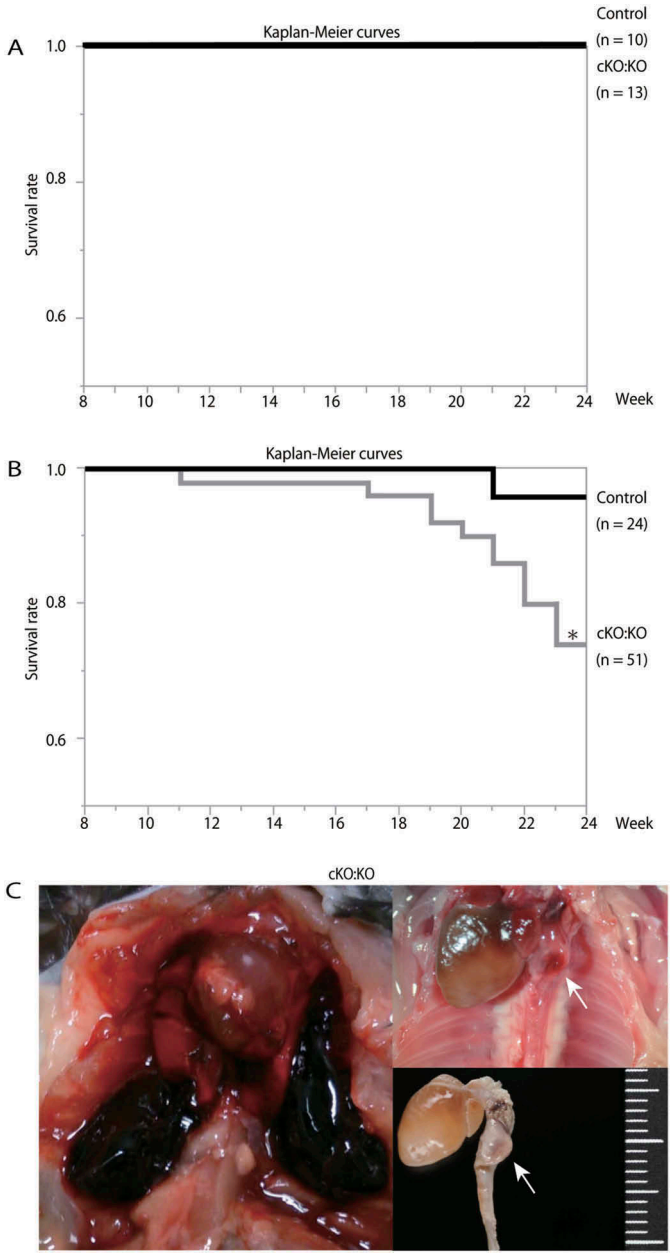

Figure 3. Survival rates of *apoeKO* mice and *Atg7cKO: apoeKO* mice fed a Western diet. (A) Kaplan-Meier curves of control *Atg7$^{f/f}$:apoeKO* mice (Control; n = 10) and *Atg7cKO:apoeKO* mice (cKO:KO; n = 13) fed a normal chow diet. (B) Kaplan-Meier curves of control *Atg7$^{f/f}$:apoeKO* mice (Control; n = 24) and *Atg7cKO:apoeKO* mice (cKO:KO; n = 51) fed a Western diet. *$P < 0.05$ vs Control. (C) Representative images upon autopsy of a *Atg7cKO:apoeKO* mice fed a Western diet. Arrows indicate cracks in the aorta.

Atg7cKO:apoeKO mice fed a Western diet showed extensive morphological changes of the media and the progression of atherosclerosis

Next, we evaluated the morphology of atherosclerotic lesions, with a focus on the suprarenal aortas of control *Atg7$^{f/f}$:apoeKO* mice and *Atg7cKO:apoeKO* mice fed a normal chow diet and a Western diet for 14 weeks (Figure 5(A)). In control *Atg7$^{f/f}$:apoeKO* mice and *Atg7cKO:apoeKO* mice fed a normal chow diet, we only occasionally found very early stage and small atherosclerotic lesions in the suprarenal aorta that were difficult to quantitate for comparison. In contrast, control *Atg7$^{f/f}$:apoeKO* mice and *Atg7cKO:apoeKO* mice fed a Western diet showed much larger atherosclerotic lesions than the same mice fed a normal chow diet (Figure 5(A)). In mice fed a Western diet, plaque sizes in the abdominal aortic region of *Atg7cKO:apoeKO* mice were significantly larger than control *Atg7$^{f/f}$:apoeKO* mice (Figure 5(B)) and these changes resulted in luminal narrowing (Figure 5(C)). Atherosclerotic lesions found in *Atg7cKO:apoeKO* mice mimic some of the features of the various stages of human atherosclerotic lesions, such as fatty streaks, which are composed of macrophage-derived foam cells (Figure 5(D)), complicated plaques with thick fibrous caps (Figure 5(E)),

Table 1. Data in control *Atg7$^{f/f}$:apoeKO* mice mice and *Atg7cKO:apoeKO* mice after 14-weeks of Western-diet load.

	Atg7$^{f/f}$:apoeKO mice	*Atg7cKO:apoeKO* mice	*P* value
Normal chow diet			
Body weight (g)	33.34 ± 1.27 (n = 10)	31.92 ± 0.97 (n = 13)	0.389
Average food consumption (g/day)	3.31 ± 0.02 (n = 10)	3.22 ± 0.08 (n = 13)	0.17
Western diet			
Body weight (g)	34.89 ± 0.98 (n = 23)	31.55 ± 0.56 (n = 34)	0.005
Average food consumption (g/day)	3.04 ± 0.49 (n = 23)	2.92 ± 0.39 (n = 34)	0.33
Mean systemic arterial pressure (mmHg)	78.3 ± 1.6 (n = 21)	77.0 ± 2.5(n = 33)	0.73
Total cholesterol (mg/dl)	834.2 ± 52.1 (n = 23)	568.3 ± 26.1 (n = 35)	0.0048
LDL cholesterol (mg/dl)	173.8 ± 9.9 (n = 23)	147.0 ± 9.7 (n = 35)	0.058
HDL cholesterol (mg/dl)	15.2 ± 0.6 (n = 23)	13.0 ± 0.5 (n = 35)	0.0075
Triglyceride (mg/dl)	33.0 ± 2.7 (n = 23)	22.7 ± 1.6 (n = 35)	0.002

Blood samples were collected from control *Atg7$^{f/f}$:apoeKO* mice and *Atg7cKO:apoeKO* mice fed a normal chow diet or a Western diet for 14 weeks. Each sample was obtained in the fasting state. Data are represented as mean ± SEM.

migration of SMCs into the sub-endothelial space in atherosclerotic plaque lesions (Figure 5(E,F)), and large areas necrotic tissue containing cholesterol crystals (Figure 5(F)). In the adventitia and perivascular tissue of *Atg7cKO:apoeKO* mice, the accumulation of infiltrated monocytes, macrophages, neutrophils, plasma cells, and fibroblasts were found (Figure 5(G)). These features of the lesions indicated chronic inflammation in the vasculature.

We further investigated the composition of the plaque lesions in control *Atg7$^{f/f}$:apoeKO* mice and *Atg7cKO:apoeKO* mice fed a Western diet. The ACTA2-positive area in the atherosclerotic plaques of *Atg7cKO:apoeKO* mice was significantly reduced compared with that of control *Atg7$^{f/f}$:apoeKO* mice (Figure 6(A,B)). The area positive for LGALS3 (lectin, galactose binding, soluble 3), a macrophage marker, was also reduced in the atherosclerotic plaques of *Atg7cKO:apoeKO* mice compared with control *Atg7$^{f/f}$:apoeKO* mice (Figure 6(C,D)). Collagen-positive area and the necrotic core area were significantly larger in *Atg7cKO:apoeKO* mice (Figure 6(E-H)). Taken together, fibrous caps of the atherosclerotic lesions of *Atg7cKO:apoeKO* mice resembled features of human atherosclerotic lesions that were almost completely composed of ACTA2-positive cells (Figure 6(A)). In addition, the thickened intima-media complex was composed of high amount of the extracellular matrix (Figure 6(G)) with relatively fewer macrophage marker-positive cells (Figure 6(D)). Intriguingly, although in general the fibrous caps were thicker in the atherosclerotic lesions of *Atg7cKO:apoeKO* mice (Table 2), in some of the advanced lesions of these mice, we found regions with thinner fibrous caps and fewer SMCs (Figure 6(A)), implying the presence of vulnerable plaques [26,27]. These data suggest that *Atg7cKO:apoeKO* mice have more advanced atherosclerotic lesions than control *Atg7$^{f/f}$:apoeKO* mice under Western diet.

Atg7cKO:apoeKO mice fed a Western diet showed increased apoptotic cell death in their plaques and media

Consistent with a previous study [28], SQSTM1-positive cells were hardly observed in control *Atg7$^{f/f}$:apoeKO* mice at the age of 10 weeks (Figure 2(B)); however, they were frequently observed not only in the plaques but also in the media, subendothelial space, and fibrous caps of control *Atg7$^{f/f}$:apoeKO* mice fed a Western diet for 14 weeks (Figure 7(A)). Furthermore, SQSTM1-positive cells were more frequently located in those places of *Atg7cKO:apoeKO* mice after 14 weeks on a Western diet (Figure 7(A)). In addition, close observation demonstrated that strong SQSTM1-positive inclusions existed within SMCs of *Atg7cKO:apoeKO* mice fed a Western diet (Figure 7(A)). Whereas cytosolic inclusions were rarely found by TEM in SMCs of control *Atg7$^{f/f}$:apoeKO* mice fed a Western diet, they were frequently observed in *Atg7cKO:apoeKO* mice fed a Western diet, particularly in the cytosol of their SMCs of the medial layer, under the plaque lesions (Figure 7(B)). TEM demonstrated that these inclusions were composed of fibrillar structures and were similar to those described previously [2,5]. Intriguingly, TEM and the TUNEL assay showed that dying SMCs were not observed in control *Atg7$^{f/f}$:apoeKO* mice fed a Western diet, but they were occasionally found in the media, on the plaque lesions of *Atg7cKO:apoeKO* mice fed a Western diet (Figure 7(B,C)). These observations were confirmed by quantitative analyses of TUNEL-positive areas of the media and plaques of these mice (Figure 7(C,D)). TEM demonstrated the presence of dying SMCs with pyknotic nuclei and the infiltration of inflammatory cells in the media of *Atg7cKO:apoeKO* mice, which were not observed in control *Atg7$^{f/f}$:apoeKO* mice (Figure 7(B)).

Atg7cKO:apoeKO mice fed a Western diet showed increased medial disruption

Atherosclerosis plaque growth is usually accompanied by compensatory outward arterial remodeling in response to shear stress alterations, in an attempt to normalize lumen diameter [29]. Autopsy of *Atg7cKO:apoeKO* mice fed a Western diet suggest that some of these mice died of aortic aneurysm rupture (Figure 3(C)). In addition, *Atg7cKO:apoeKO* mice fed a Western diet showed larger maximal external diameters of the suprarenal aorta than control *Atg7$^{f/f}$:apoeKO* mice (Figure 4(B)), suggesting that compensatory outward remodeling occurred. Thus, we evaluated the morphological changes associated with aneurysm formation and rupture.

Whereas the loss of medial SMCs leads to arterial remodeling [29], we found that ACTA2-positive area was reduced not only in individual plaques but also in the media of *Atg7cKO:apoeKO* mice (Figure 6(A)). In addition, although the number of LGALS3-positive cells was smaller in atherosclerotic plaques, accumulation of monocytes and macrophages were found in the media and adventitia of *Atg7cKO:apoeKO* mice fed a Western

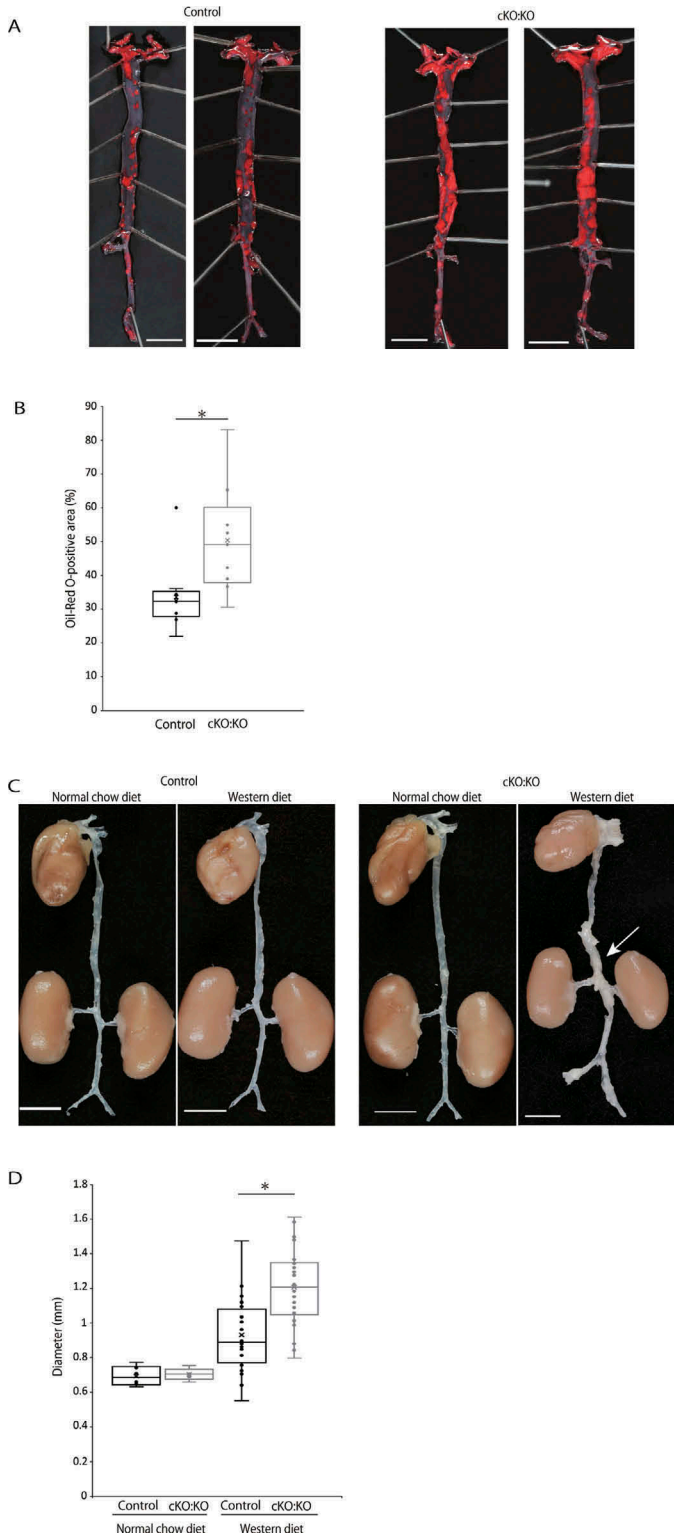

Figure 4. Autophagy deficiency accelerates atherosclerosis and increases maximal external diameter in SMCs of mice fed a Western diet. (A) Representative en face view of the entire aorta of control *Atg7*$^{f/f}$*:apoeKO* mice (Control) and *Atg7cKO:apoeKO* mice (cKO:KO) fed a Western diet, stained with oil-red O. Scale bars: 5 mm. (B) Oil-red O-positive areas of Control and cKO:KO fed a Western diet. Data are shown as a box plot of 9 mice in each group. *$P < 0.05$ vs Control. (C) Representative view of the entire aorta of Control and cKO:KO fed either a normal chow diet or a Western diet. The white arrow indicates the suprarenal aorta with an enlarged diameter. Scale bars: 5 mm. (D) Maximal external diameters of the suprarenal aorta of Control and cKO:KO fed a normal chow diet or a Western diet. Data are shown as a box plot of 6 Control and 5 cKO:KO fed a normal chow diet and 20 Control and 30 cKO:KO fed a Western diet. *$P < 0.05$ vs Control.

diet (Figure 6(C)). A previous study demonstrated that the apoptosis of SMCs attracted inflammatory cells, including monocytes, macrophages, and leukocytes, in part through the production of CCL2 (chemokine [C-C motif] ligand 2), leading to aneurysm formation [30]. Thus, we next analyzed the expression of CCL2. CCL2-positive area in *Atg7cKO:apoeKO* mice were larger than that in control *Atg7*$^{f/f}$*:apoeKO* mice in the media (Figure 8(A,B)), and adventitia and perivascular tissue (Figure 8(A,C)). In particular, not only CCL2-positive macrophages but also CCL2-positive SMCs were found in the media and the adventitia. Thus, an increased local expression of CCL2 may be associated with the recruitment of monocytes and macrophages in the media, adventitia, and perivascular tissue in *Atg7cKO:apoeKO* mice fed a Western diet.

Elastin, which is one of the main components of the media in the aortic wall, maintains the tensile strength and structural integrity of the vascular wall. The fragmentation of elastic fibers is one of the most notable features of aneurysm formation [31]. Thus, we assessed breaks in the lamina of *Atg7cKO:apoeKO* mice fed a Western diet. As shown in Figure 8(D,E), the number of lamina breaks were significantly increased in *Atg7cKO:apoeKO* mice fed a Western diet compared with control *Atg7*$^{f/f}$*:apoeKO* mice. In particular, these lesions were found almost exclusively at the proximal portion of atherosclerotic plaques. Importantly, local saccular aneurysm-like dilatations were seen in several regions, only in *Atg7cKO:apoeKO* mice fed a Western diet, where medial disruption was observed (Figure 8(F)).

Accumulating lines of evidence suggest that matrix metalloproteinase-9 (MMP9), which is a member of the matrix metalloproteinases, is associated with abdominal aortic aneurysms through cleaving ELN (elastin) and degrading collagen fragments [32,33]. MMP9-positive areas in *Atg7cKO:apoeKO* mice were larger than those in control *Atg7*$^{f/f}$*:apoeKO* mice in the media (Figure8(G,H)), and adventitia and perivascular tissue (Figure 8(G,I). However, very few MMP9-positive SMCs were observed in the media and adventitia of *Atg7cKO:apoeKO* mice. However, infiltrated monocytes, macrophages, neutrophils, plasma cells, and fibroblasts were accumulated in those areas (Figure 5(G)), suggesting that these cells may be the main source of MMP9 production.

Autophagy-deficient SMCs are susceptible to 7-ketocholesterol (7-KC)-induced apoptotic cell death and CCL2 expression

Atg7cKO:apoeKO mice showed a progression of atherosclerosis with outward arterial remodeling only when fed a Western diet. Our data suggest that enhanced apoptotic cell death and CCL2 expression in SMCs may play a key role in this phenotype. Thus, we investigated the effect of the atherogenic cholesterol 7-KC, which is a component of oxidized low-density lipoprotein-cholesterol, on the SMCs isolated from *Atg7cKO* mice. Although there were no differences in cleaved CASP3 (caspase 3) levels between SMCs from control *Atg7*$^{f/f}$ mice and SMCs from *Atg7cKO* mice, 7-KC increased cleaved CASP3 levels in both types of SMCs. The effect of 7-KC on cleaved CASP3 in SMCs of *Atg7cKO* mice is higher than in SMCs of control *Atg7*$^{f/f}$ mice (Figure 9(A)). In addition, 7-KC induced higher expression

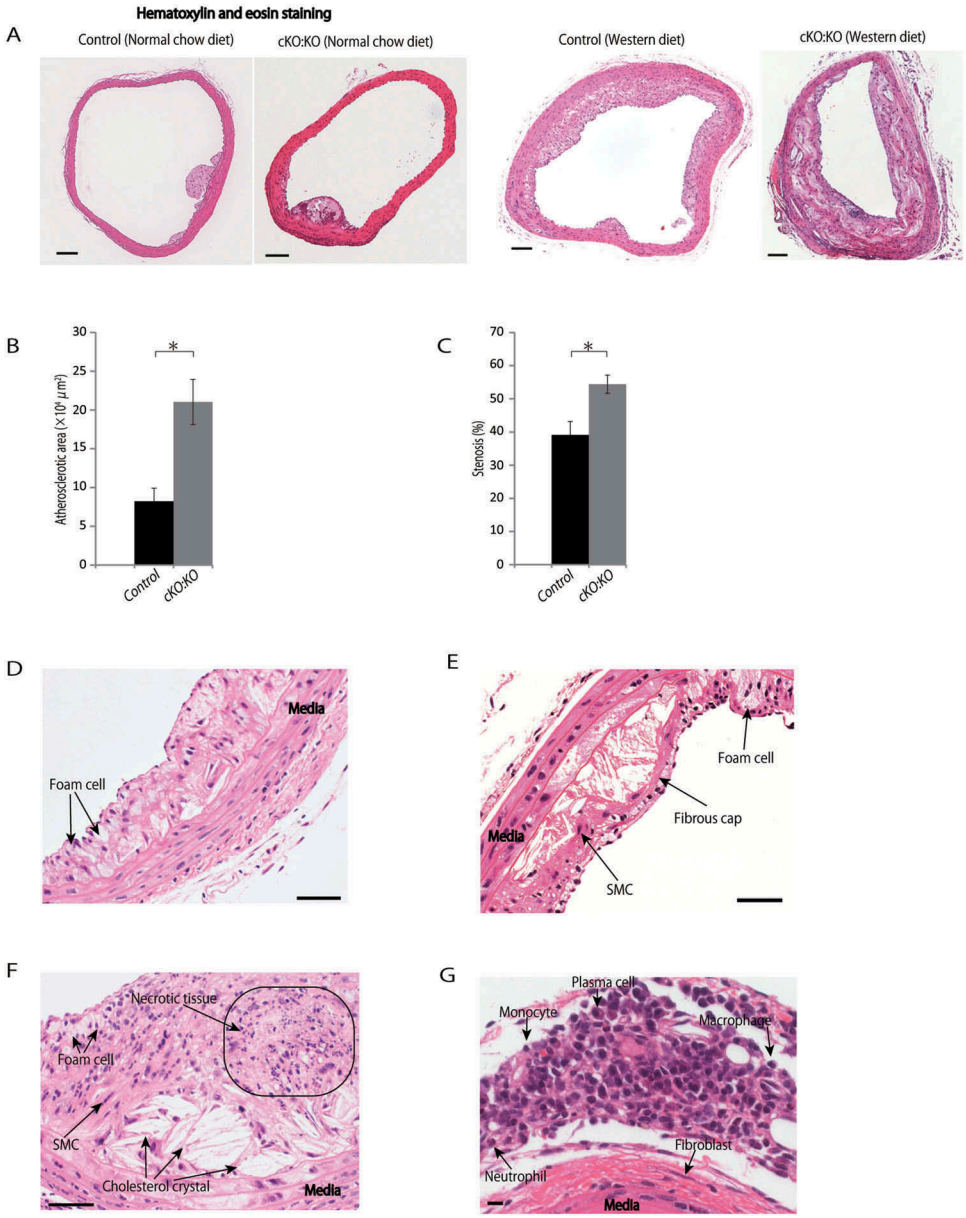

Figure 5. Morphological changes of atherosclerotic lesions in *Atg7cKO:apoeKO* mice fed a Western diet. Atherosclerotic lesions of control *Atg7$^{f/f}$:apoeKO* mice (Control) and *Atg7cKO:apoeKO* mice (cKO:KO) fed a normal chow diet or a Western diet for 14 weeks were evaluated. (A) Representative histological sections of abdominal aortas stained with hematoxylin and eosin of Control and cKO:KO fed a normal chow diet and Western diet. (B) Percentage atherosclerotic areas of the aortas of Control and cKO:KO fed a Western diet. Data are shown as the mean ± SEM of 11 Control and 21 cKO:KO mice. *$P < 0.05$ vs Control. (C) Percentage luminal stenosis of Control and cKO:KO fed a Western diet. Data are shown as the mean ± SEM of 11 Control and 21 cKO:KO. *$P < 0.05$ vs Control. (D, E and F) Atherosclerotic lesions of cKO:KO fed a Western diet. Scale bars: 50 μm. (G) Adventitia and the perivascular tissue of an atherosclerotic lesion of cKO:KO fed a Western diet. Scale bar: 10 μm.

levels of H2AFX and higher phosphorylation levels of TRP53 in SMCs from *Atg7cKO* mice than SMCs from control *Atg7$^{f/f}$* mice. In addition, *Atg7cKO* mice demonstrated stronger senescence-associated GLB1 staining than that of control *Atg7$^{f/f}$* mice (Figure 9(B,C)). Along with increased susceptibility to apoptosis and senescence caused by 7-KC exposure, the expression levels of CCL2 in SMCs from *Atg7cKO* mice were significantly higher than those in SMCs from control *Atg7$^{f/f}$* mice (Figure 9(A)). These data showed that in SMCs from *Atg7cKO* mice, apoptotic cell death, cellular senescence, and CCL2 expression were cell-autonomously enhanced by 7-KC exposure.

Discussion

This study supports the importance of autophagy in SMCs for protection against the progression of atherosclerosis, adding further evidence to recent studies [17,18]. We found that not only the progression of atherosclerosis with enhanced SMC death, but also arterial outward remodeling with increased lamina breaks appeared to be associated with the increased frequency of aortic aneurysm rupture in *Atg7cKO:apoeKO* mice fed a Western diet. We demonstrated the important role of SMC autophagy in preventing aortic aneurysm rupture. In addition, we showed that *Atg7cKO:apoeKO* mice fed a

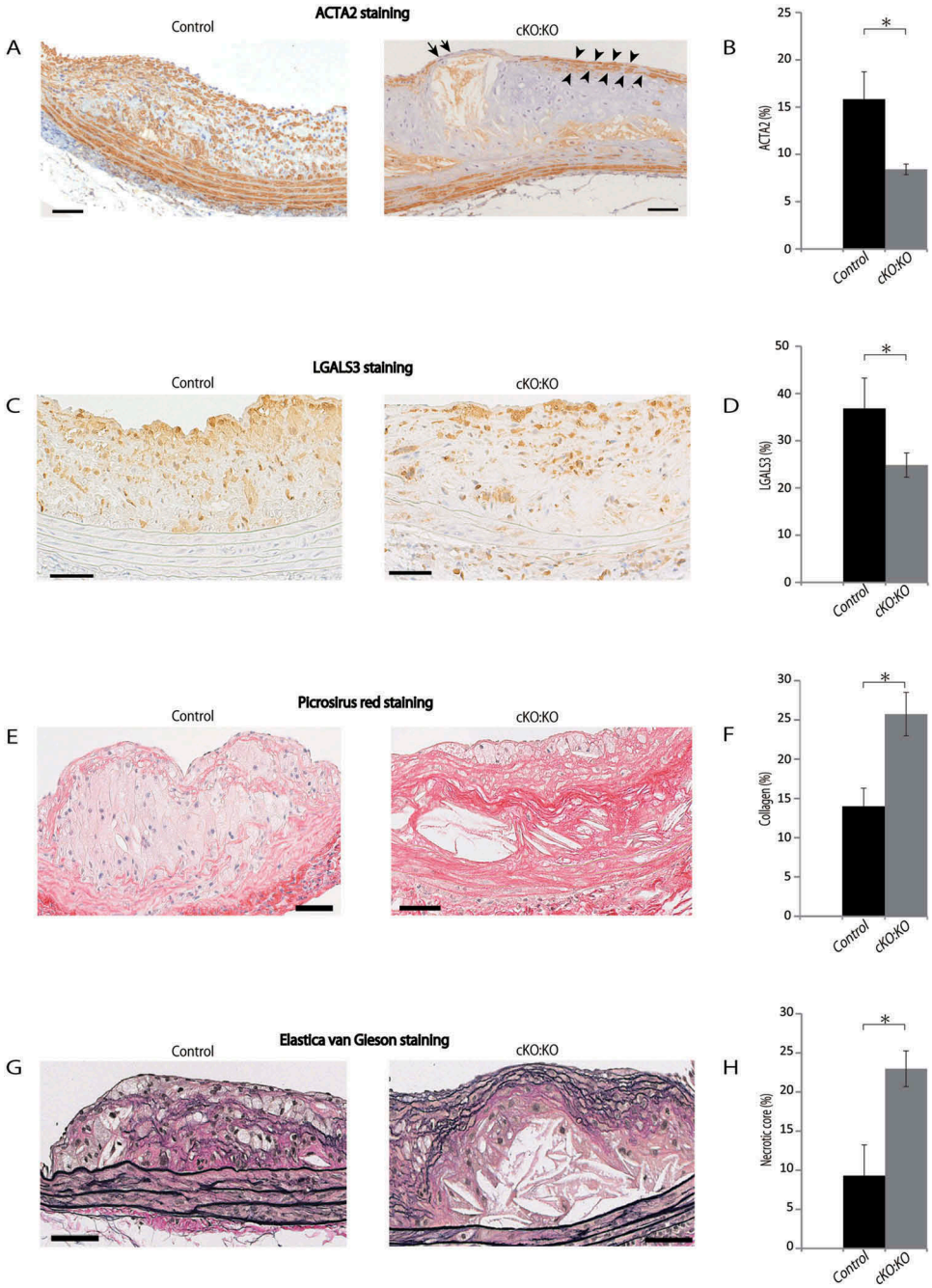

Figure 6. Composition of atherosclerotic lesions of *Atg7cKO:apoeKO* mice fed a Western diet. (A) Representative histological images of abdominal aortic plaques of *Atg7*$^{f/f}$*: apoeKO* mice (Control) and *Atg7cKO:apoeKO* mice (cKO:KO) fed a Western diet for 14 weeks, stained with an ACTA2 antibody. The area between the arrowheads indicates a fibrous cap. Arrows indicate the thin fibrous cap. Scale bars: 50 μm. (B) Areas of ACTA2-positive regions in the abdominal aortic plaques. Data are shown as the mean ± SEM of 11 Control and 21 cKO:KO. *P < 0.05 vs Control. (C) Representative histological images of abdominal aortic plaques from Control and cKO:KO stained with LGALS3 antibody from Control and cKO:KO. Scale bars: 50 μm. (D) The area of LGALS3-positive regions in the abdominal aortic plaque was evaluated. Data are mean ± SEM of 11 Control and 21 cKO:KO each. *P < 0.05 vs Control. (E) Representative histological images of abdominal aortas from Control and cKO:KO stained with Picrosirius red. Scale bars: 50 μm. (F) Collagen contents area was evaluated. Data are mean ± SEM of 11 Control and 21 cKO:KO each. *P < 0.05 vs Control. (G) Representative histological images of abdominal aorta stained with Elastica van Gieson staining from Control and cKO:KO. Scale bars: 50 μm. (H) Necrotic core area was evaluated. Data are mean ± SEM of 11 Control and 21 cKO:KO each. *P < 0.05 vs Control.

Western diet is a mouse model that develops aortic aneurysm ruptures without using any special agents.

Grootaert et al. demonstrate that SMC-specific *Atg7* deficiency promotes diet-induced atherogenesis [18]. In that study, SMC-specific *Atg7*-deficient mice are more resistant to oxidative stress-induced cell death, and result in increased cell size, total collagen amount, migration capacity, and senescence, and a decrease in proliferation capacity *in vitro*. Consistent with these findings, we also found that SMCs isolated from *Atg7cKO* mice demonstrated no significant increase in cell death after 24 h of culture, and demonstrated resistance to exogenous high oxidative stress-induced cell death, increased senescence, and decreased proliferation capacity *in vitro*. In addition, we provided novel findings regarding the effect of 7-KC. Although *Atg7* deficiency in SMCs showed resistance to oxidative stress-induced cell death, these cells

Table 2. Minimum, maximum and mean cap thickness in control *Atg7$^{f/f}$:apoeKO* mice and *Atg7cKO:apoeKO* mice after 14-weeks of Western diet.

	Atg7$^{f/f}$:apoeKO mice	*Atg7cKO:apoeKO* mice	*P* value
Minimum fibrosis cap thickness	4.9 ± 2.8(n = 11)	7.4 ± 0.7 (n = 23)	0.035
Maximum fibrosis cap thickness	32.1 ± 7.0 (n = 11)	52.5 ± 7.3 (n = 23)	0.058
Mean fibrosis cap thickness	13.6 ± 1.6 (n = 11)	22.5 ± 2.6 (n = 23)	0.002

Data are represented as mean ± SEM.

were more susceptible to 7-KC-induced cell death accompanied by activation of the TRP53 pathway (Figure 9(A)). Thus, the role of autophagy in the apoptosis of SMCs may vary depending on the stimuli. Given that enhanced apoptosis was observed in *Atg7cKO:apoeKO* mice fed a Western diet (Figure 7), the phenomenon observed in *in vitro* cultures of SMCs with 7-KC may reflect the *in vivo* findings.

Regarding *in vivo* studies, Grootaert et al. find that SMC-specific *Atg7* deficiency in *apoeKO* mice accelerates atherosclerotic plaque formation with increased cell death, necrotic lesion size, plaque macrophages, fibrous cap thickness, collagen content, and SMC senescence after being fed a Western diet for 10 weeks. However, plaque size, necrotic lesion size, and apoptotic cell number are no longer increased after 14 weeks on a Western diet, although fibrous cap thickness and collagen content are still increased in *apoeKO* mice deficient in *Atg7* specifically in SMCs [18]. In contrast, we found that plaque sizes in the abdominal aortic area of *Atg7cKO:apoeKO* mice fed

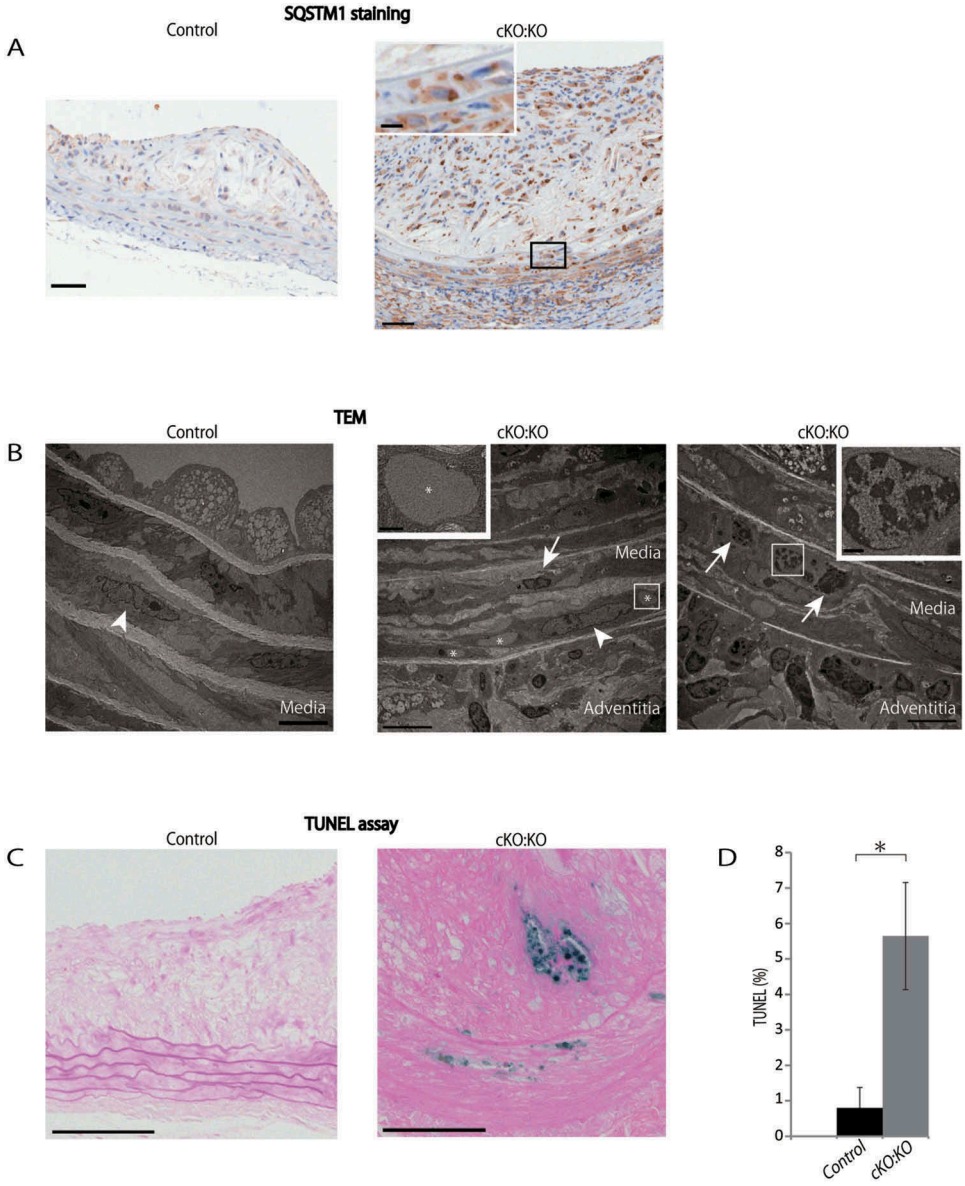

Figure 7. *Atg7cKO:apoeKO* mice under Western diet shows increased apoptotic cell death in plaque and media. (A) Representative histological images of abdominal aorta stained with SQSTM1 antibody from control *Atg7$^{f/f}$:apoeKO* mice (Control) and *Atg7cKO:apoeKO* mice (cKO:KO) fed a Western diet. Scale bars: 50 μm. (B) Transmission electron microscopy (TEM) images of abdominal aorta from Control and cKO:KO under Western diet. The asterisks indicate cytosolic inclusions. The white arrowheads indicate SMC nuclei with normal morphology. The boxed areas indicate dying SMCs of cKO:KO with pyknotic nuclei, and their enlarged images are shown in the insets. The white arrow indicates inflammatory cell infiltration into the media. Scale bars: 1 μm in the upper panel, and 50 μm in the lower panel. (C) Representative images of the TUNEL assay and Red Counterstain C staining of the abdominal aorta of Control and cKO:KO fed a Western diet. Scale bars: 50 μm. (D) The area of TUNEL-positive lesions in the media and plaques of the abdominal aorta was evaluated. Data are mean ± SEM of 11 Control and 21 cKO:KO each. *$P < 0.05$ vs Control.

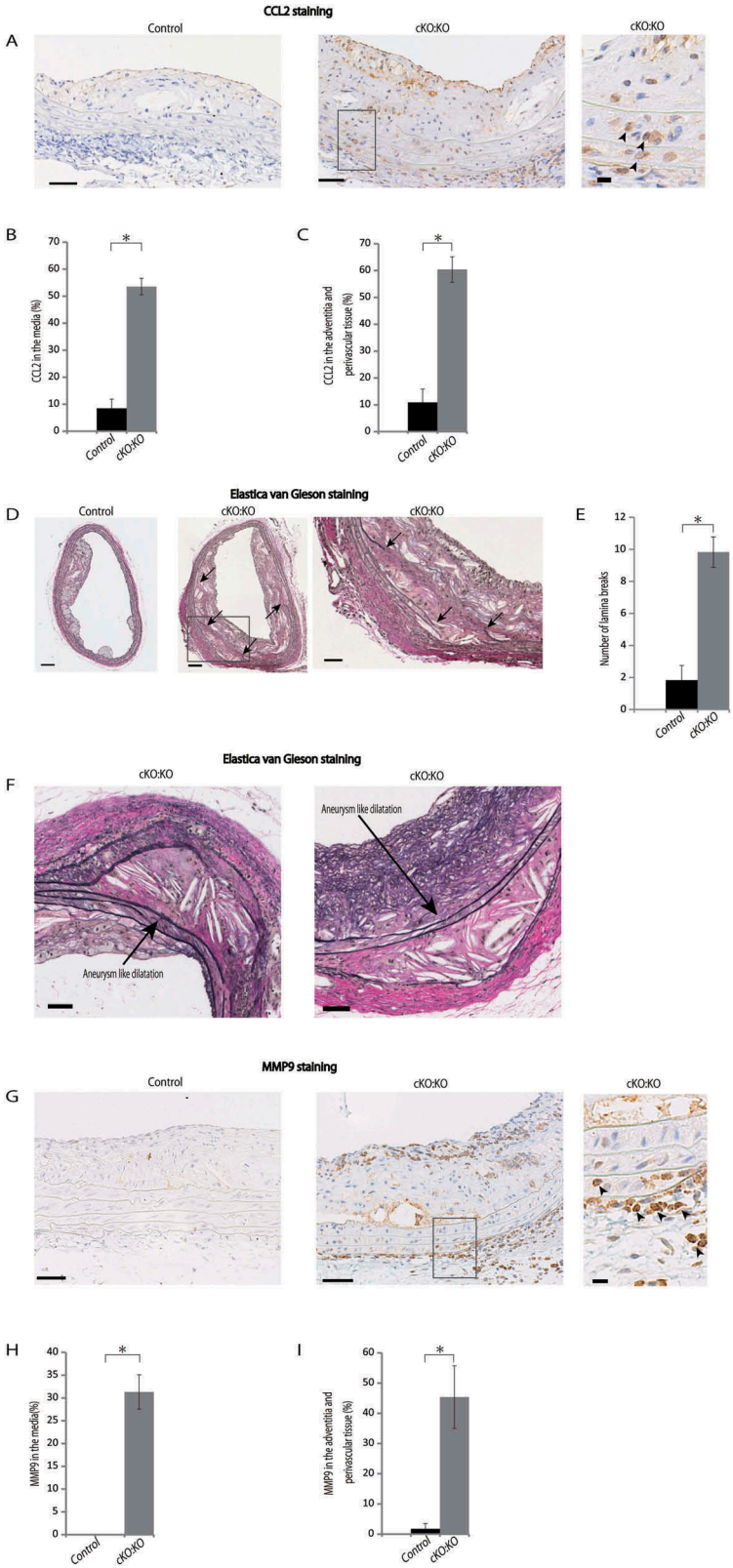

Figure 8. *Atg7cKO:apoeKO* mice under Western diet showed increased number of lamina breaks. (A) Representative histological sections of abdominal aorta stained with CCL2 from control *Atg7*$^{f/f}$*:apoeKO* mice (Control) and *Atg7cKO:apoeKO* mice (cKO:KO) fed a Western diet. Scale bars: 50 μm. An enlarged view of the boxed area is shown on the right. arrowheads indicate CCL2-positive cells. Scale bars: 10 μm.(B) The percentage of CCL2-positive cells in the media were evaluated. Data are mean ± SEM of 4 Control and 7 cKO:KO each. *$P < 0.001$ vs Control. (C) The percentage of CCL2-positive cells in the adventitia and perivascular tissue were evaluated. Data are mean ± SEM of 4 Control and 7 cKO:KO each. *$P < 0.001$ vs Control. (D) Representative histological sections of abdominal aorta from Control and cKO:KO stained with Elastica van Gieson. Scale bars: 100 μm. Enlarged view of the boxed area is shown on the right.Arrows indicate the area of lamina breaks. Scale bars: 50 μm. (E) The number of lamina breaks was evaluated. Data are mean ± SEM of 11 Control and 21 cKO:KO each. *$P < 0.05$ vs Control. (F) Representative of abdominal aorta stained with Elastica van Gieson staining from Control and cKO:KO. Scale bars: 50 μm.GRepresentative histological sections of abdominal aorta stained with MMP9 from Control and cKO:KO fed a Western diet. Scale bars: 50 μm. An enlarged view of the boxed area is shown on the right. arrowheads indicate MMP9-positive cells. Scale bars: 10 μm. (H) The percentage of MMP9-positive cells in the media were evaluated. Data are mean ± SEM of 4 Control and 5 cKO:KO each. *$P < 0.01$ vs Control. (I) The percentages of MMP9-positive cells in the adventitia and perivascular tissue were evaluated. Data are mean ± SEM of 4 Control and 5 cKO:KO each. *$P < 0.05$ vs Control.

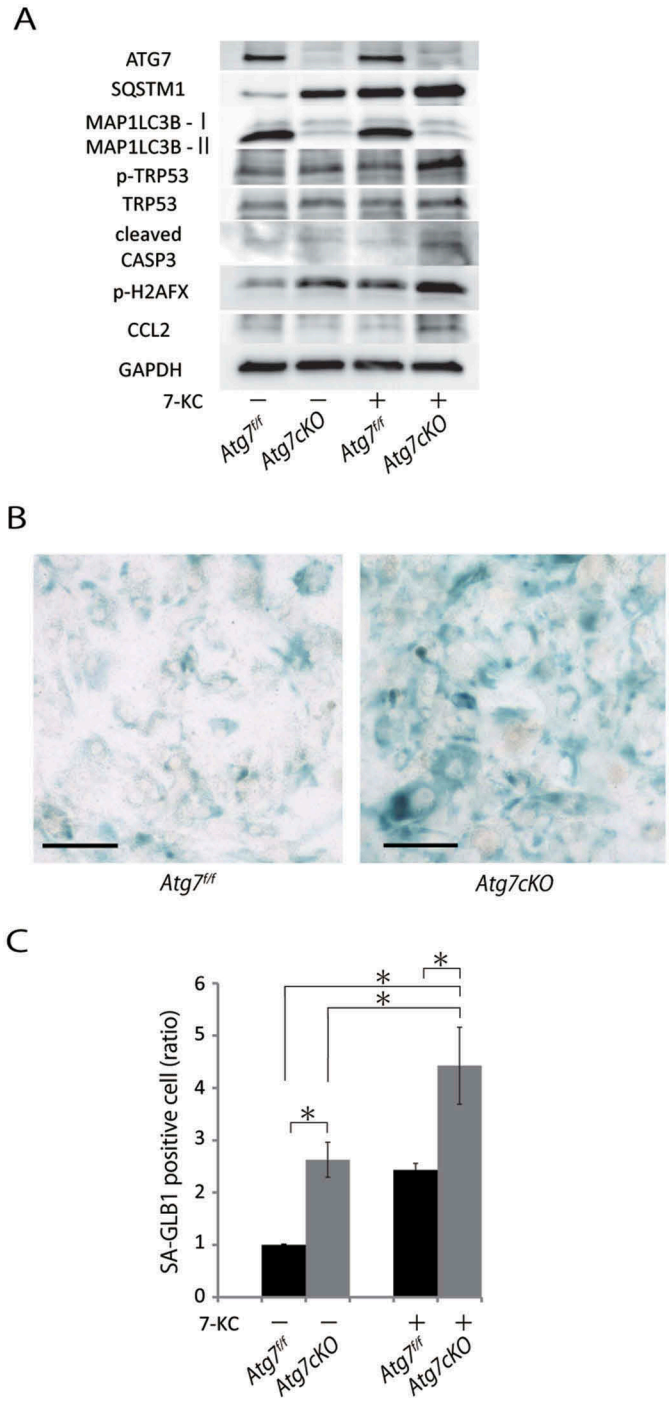

Figure 9. Autophagy-deficient SMCs are susceptible to 7-KC-induced apoptotic cell death and CCL2 expression. SMCs from control *Atg7*$^{f/f}$ and *Atg7cKO* mice at 10 weeks of age were isolated and exposed to 7-KC 20μM for 16 h. (A) Western blot analysis of primary isolated SMCs for ATG7, SQSTM1, MAP1LC3B-I, MAP1LC3B-II, TRP53, cleaved CASP3, phospho-H2AFX and CCL2. Representative results from 3 independent experiments are shown. (B) Senescence-associated GLB1 staining of SMCs. Scale bars: 300 μm. (C) Relative number of SMCs stained with senescence-associated GLB1. Data are shown as the mean ± SEM of 4 independent experiments. *$P < 0.05$ vs control *Atg7*$^{f/f}$ mice. Data from control SMCs that were not exposed to 7-KC was set to 1.0.

a Western diet were increased, together with an increase in the necrotic cores, number of apoptotic cells, fibrous cap thickness (although thinner fibrous caps were observed in some advanced lesions), and reduction of the ACTA2-positive area and plaque macrophages. In addition, we demonstrated novel findings that *Atg7cKO:apoeKO* mice had an increased number of lamina breaks and morphological changes associated with aneurysm formation and rupturing, leading to reduced survival. Although the reason for these discrepancies is not clear, it may be owing to differences in the diet used for the experiments (1.25% cholesterol plus 0.5% sodium cholate in this study vs. 0.2% cholesterol in the previous study), arteries used for evaluation (thoracic and abdominal arteries in this study vs. brachiocephalic artery and aortic root in the previous study) and control mice (*Atg7*$^{f/f}$ vs. *Atg7*$^{f/f}$ *Cre*$^{+}$). In addition, differences of intestinal bacterial flora in the mice of the 2 studies must be taken into consideration.

A previous study demonstrates that in advanced atherosclerotic plaques of humans, TUNEL-positive SMCs, macrophages, and endothelial cells are occasionally observed [8]. On the one hand, similar to previous reports in mice [8,10], control *apoeKO* mice demonstrated a very low number of TUNEL-positive cells in atherosclerotic plaques. These observations suggest different pathological changes in atherosclerotic lesions between mice and humans. On the other hand, in *Atg7cKO:apoeKO* mice, TUNEL-positive areas were widely observed not only within atherosclerotic plaques but also in the media with a significant reduction in ACTA2-positive areas. Notably, TUNEL-positive areas were found even in *Atg7cKO:apoeKO* mice at 10 weeks of age. Thus, autophagy deficiency in SMCs may result in increased cell death, probably predominantly in SMCs, and this cell death may be involved in the progression of atherosclerosis, which may share some features with human atherosclerotic lesions. Given that autophagy deficiency results in the increased apoptosis of invariant natural killer cells [34], autophagy deficiency may result in a cell-type specific enhancement of apoptosis.

In this study, SMC death by autophagy deficiency was associated with plaque growth. Regarding the causal association, a previous study demonstrates that chronic apoptosis in SMCs is sufficient to promote atherosclerosis with marked fibrous cap thinning, expansion of the necrotic core, increased calcification, and increased medial degeneration [10]. These features appear to be similar to the atherosclerotic lesions observed in *Atg7cKO:apoeKO* mice fed a Western diet. In addition, SMC apoptosis was shown to cause an increased release of inflammatory cytokines, leading to the expansion of atherosclerotic plaques through recruiting monocytes and macrophages into atherosclerotic lesions, particularly at the initial stages of atherosclerosis [9,10,35]. In contrast, the accumulation of macrophages at advanced stages of atherosclerosis in *Atg7cKO:apoeKO* mice was less than that of control *Atg7*$^{f/f}$*:apoeKO* mice, consistent with a previous report on enhanced atherosclerosis caused by chronic apoptosis in SMCs [10]. A decreased accumulation of macrophages may reflect an increase in macrophage cell death, resulting in an increase in the necrotic core. Whereas autophagy deficiency in SMCs demonstrated some features of plaque vulnerability, such as an enlarged necrotic core and a reduced fibrous cap in some places, increased SMC death may also contribute to a reduced ability to synthesize extracellular matrix proteins, leading to increased plaque vulnerability. Thus, SMC death caused by autophagy deficiency in SMCs may possibly promote the progression of atherosclerosis.

We found that the reduction in the density of SMCs by a deficiency of SMC autophagy may be associated with increased monocyte and macrophage accumulation in the media and adventitia, number of lamina breaks, and compensatory outward remodeling. The loss of medial SMCs may reduce the ability of the media to synthesize matrix proteins, leading to medial vulnerability. In addition, we found that SMCs from *Atg7cKO* mice are susceptible to enhanced CCL2 expression with enhanced phosphorylation of TRP53 by 7-KC, whereas CCL2 expression [27]. Indeed, CCL2-positive SMCs were increased in the media of *Atg7cKO:apoeKO* mice fed a Western diet. Taken together, CCL2 expression via enhanced cellular senescence induced by autophagic failure and the exposure of atherogenic lipids appeared to trigger the accumulation of monocytes and macrophages in the vascular wall (Figures 6(C) and 7(B)). Furthermore, given that elastic fibers are degraded by proteolytic enzymes, including MMP9, that were produced from the infiltrated macrophages, we observed an increased number of MMP9-positive macrophages in the media, adventitia, and perivascular tissue of *Atg7cKO:apoeKO* mice fed a Western diet (Figure 8). Accordingly, these molecules appear to be involved in the susceptibility of the formation and rupture of aneurysms in *Atg7cKO:apoeKO* mice fed a Western diet.

Although the medial vulnerability and the fragmentation of elastic fibers are considered as the most important features of the wall in the process of aneurysm formation [31], we found only a few lesions of local saccular aneurysm-like dilatations. This result suggests that alterations in hemodynamic features, such as increased blood pressure, may be required to promote the formation of advanced aneurysms as well as their rupture. In this regard, autophagy deficiency in SMCs did not contribute to the increase in blood pressure, consistent with a recent report [17]. Notwithstanding, it should be noted that lesions of local saccular aneurysm-like dilatations were rarely found in control $Atg7^{f/f}$*:apoeKO* mice that did not receive any stimuli, suggesting that SMC autophagy plays a crucial role in maintaining medial strength. Conversely, although *Atg7cKO:apoeKO* mice fed a Western diet may be used as a model of aortic aneurysm without requiring any special agents, regarding their phenotypic predictability, the widely used AGT II/angiotensin II fusion model maybe a more reliable model [36].

In conclusion, we demonstrated that autophagy deficiency in SMCs promotes atherosclerosis at least in part through SMC death. Based on the possible implication of SMC autophagy, the induction of autophagy may be a potential novel therapeutic strategy against the progression of atherosclerosis.

Materials and methods

Animals

The study protocol was reviewed and approved by the Animal Care and Use Committee of Juntendo University. *apoe*-null mice and $TaglnCre^{+/0}$ mice purchased from the Jackson Laboratory were housed in specific pathogen-free barrier facilities. $Atg7^{f/f}$ mice [37] were bred with $TaglnCre^{+/0}$ mice to generate mice homologous for the floxed allele and hemizygious for the *Cre* transgene (*Atg7cKO*), as smooth muscle-specific *Atg7*-deficient mice (backcrossed at least 10 times on a C57BL/6 background). Littermate controls were homozygous for the floxed allele *Atg7* gene, but did not carry the *Cre* transgene ($Atg7^{f/f}$) [38]. Then, *Atg7cKO* and *apoeKO* mice (C57BL/6 background) were bred to generate *Atg7cKO:apoeKO* mice and control $Atg7^{f/f}$*:apoeKO* mice used for this study (Charles River, Ishioka, Ibaraki, Japan). Mice were maintained under a 12-h light/dark cycle, and fed a standard rodent diet (22.6% protein, 53.8% carbohydrate, 5.6% fat, 6.6% mineral and vitamin mixture, and 3.3% fiber; total: 356 kcal/100 g, CRF-1, Charles River Japan) with water ad libitum. At the age of 10 weeks, mice were continued to be fed a normal chow diet or were fed a Western diet (1.25% cholesterol, 15% fat, and 0.5% sodium cholate) (EPS EKISHIN Co., D12108C) which promotes atherosclerosis in mice.

Laboratory data

Blood samples were collected when the mice were sacrificed. The concentrations of cholesterol, triglyceride, chylomicron, very-low-density lipoprotein, low-density-lipoprotein cholesterol, and high-density-lipoprotein cholesterol were measured by Skylight Biotech, Inc. (Tokyo, Japan).

Blood pressure measurements

Blood pressure (BP) was measured by a non-invasive tail-cuff method using a Model UR-5000 system (Ueda Co., Tokyo, Japan). For BP measurements, mice were placed in a warm mouse restraining apparatus. A cuff was placed around the tail and inflated until blood flow was occluded, and then released. The first pulses of arterial flow that were detected were recorded as systolic and diastolic BP. Three BP measurements were performed at the end of the study and BP was determined for each animal by averaging the obtained values. The mean systolic and diastolic BP was used for representing the BP as mean systemic arterial pressure.

Cell culture

Murine aortic SMCs were isolated and cultured as previously described [39]. Mouse aortic SMCs were maintained in Dulbecco Modified Eagle Medium containing 20% fetal bovine serum (FBS), 100 units/mL penicillin, 100 μg/mL streptomycin, 2.5 μg/mL amphotericin B, and 400 μg/mL L-glutamine. Cells were used between passages 3 and 7 for the experiments and individual experiments were repeated at least 3 times with different preparations of cells. The medium was changed every 48 h. For the experiments, SMCs were plated on 6-well plates at 10×10^4 cells per well. Cell number counts were performed using a hemocytometer on days 2, 4, 6, and 8.

Quantification of atherosclerotic lesions

The aorta was flushed with normal saline followed by 10% buffered formalin, as described previously [40–42]. The aorta was excised from the root to the common iliac artery. Then, the

connective and adipose tissues were removed from the aorta and the entire aorta was stained with oil red O (MUTO PURE CHEMICALS CO.,LTD, Tokyo, Japan, 40,491). Images were captured with a digital single-lens reflex camera and maximal diameters of the suprarenal abdominal aorta were measured with ImagePro Plus software. The percentage of oil red O-positive area was calculated by dividing oil red O-positive areas by the area of the entire aorta (from the ascending aorta to the right suprarenal artery). For quantitative analysis of atherosclerotic lesions, the aneurysm and atherosclerosis-prone suprarenal portion of the abdominal aorta was embedded in optimal cutting temperature compound, then 4-μm thick cross-sections at 50-μm intervals were prepared with a cryostat. Twelve consecutive sections were taken sequentially, allowed to dry at room temperature for 30 min, and stained with hematoxylin & eosin (MUTO PURE CHEMICALS CO.,LTD, 32042, 30022), Elastica van Gieson (MUTO PURE CHEMICALS CO., LTD, 40322,40341,40351,40362,40372), or Picrosirius red stain (Polysciences, Inc., 24901–250) to evaluate atherosclerotic area. Then, immunohistochemistry was performed using a rat anti-mouse or human LGALS3/MAC-2 monoclonal antibody (Cedarlane Laboratories Ltd., CL8942AP), mouse anti-human ACTA2/α-SMA antibody (Dako, M0851), guinea pig anti-human SQSTM1/p62 polyclonal antibody (Progen Biotechnik GmbH, GP62-C), rabbit anti-PCNA antibody (Santa Cruz Biotechnology, sc-7907), rabbit anti-CCL2/MCP-1 (Abcam, ab7202), or rabbit anti-MMP9 (Abcam, ab38898). The TUNEL assay was performed using VasoTACS™ *in situ* Apoptosis detection kit (TREVIGEN Inc., 4826–30-K) including Red Counterstain C, an acidophilic cytoplasmic countrstain (TREVIGEN Inc., 4800–30-19),according to the manufacturer's instructions. The percentage of ACTA2-positive area, LGALS3-positive area, necrotic core defined as the area including cholesterol crystals and surrounding necrotic products analyzed by staining with hematoxylin and eosin, collagen-positive area analyzed by staining with the Picrosirius red stain and TUNEL-positive area were calculated by each area divided by the atherosclerotic area. The percentage of CCL2- or MMP9-positive cells were calculated by dividing CCL2- or MMP9-positive cells by the total number of cells in the field of lesion examined. The percentage of cross-sectional stenosis area was calculated by dividing the area of the non-occluded region of the lumen by the area of the region inside the outer layer of the tunica media. The medial lamina breaks were defined as apparent gaps in the continuity of elastic lamina upon Elastica van Gieson staining. Images were captured with ImagePro Plus software. The number of immunopositive cells were counted using 3 images per animal.

Electron microscopy

TEM analyses were performed as previously described [5]. Briefly, primary SMCs and mice were fixed by immersion and cardiac perfusion, respectively, with 2% glutaraldehyde in 0.1 mol/L PB (pH 7.4) (LSI Medience Corporation, RM102-5L). Samples were embedded in epoxy resin. Semi-thin sections were cut and stained with toluidine blue. Ultrathin sections (80 nm thick) were cut and observed with a Hitachi HT7700 electron microscope (Hitachi, Tokyo, Japan).

Preparation of cells and Western blot analysis

To assess the effect of oxidative stress, SMCs were pretreated with or without the antioxidant N–acetylcysteine (NAC; Sigma-Aldrich, A9165) at 10 mM for 10 min, and then were cultured for up to 48 h. With respect to assessing the effect of atherogenic cholesterol, SMCs were exposed to 7-ketocholesterol (7-KC; Sigma-Aldrich, C2394) for up to 16 h. All samples were sonicated on ice and centrifuged at 15,000 × *g* at 4°C for 15 min. The supernatants were subjected to Western blot analysis using primary antibodies, as follows: guinea pig anti-human SQSTM1/p62 antibody (Progen Biotechnik GmbH, GP62-C), rabbit anti-MAP1LC3B/LC3 antibody (Sigma-Aldrich, L7543), mouse anti-TRP53 (1C12) antibody (Cell Signaling Technology, 2524), rabbit anti-phospho-TRP53 (Ser15) antibody (Cell Signaling Technology, 9284), rabbit anti-BBC3/PUMA antibody (Cell Signaling Technology, 7467), rabbit anti-phospho-H2AFX antibody (ser1339) (Cell Signaling Technology, 9718), rabbit anti-ATG7 antibody [43], rabbit anti-GAPDH (glyceraldehyde-3-phosphate dehydrogenase) antibody (Cell Signaling Technology, 2118), rabbit anti-cleaved CASP3 (Cell Signaling Technology, 9661), and rabbit anti-CCL2/MCP-1 (Cell Signaling Technology, 2029) as described previously [40,42].

Cell death detection by enzyme-linked immunosorbent assay (ELISA)

Cells were incubated for 48 h in 96-well plates with medium containing 20% FBS with or without 10 mM NAC, centrifuged at 200x g for 10 min, and the supernatants were separated. The cell pellets were treated with lysis buffer for 30 min and centrifuged again. The cell lysates and supernatants were used for the cell death assay using a Cell Death Detection Kit (Roche Diagnostics, 11774425001) to detect histone-associated DNA fragments (mononucleosomes and oligonucleosomes) in the cytoplasm and released from the cell, by a photometric enzyme immunoassay according to the manufacturer's protocol.

Analysis of cell senescence

SMCs were plated at a density of 10×10^4 cells/well in 6-well culture plates with complete media and cultured for 48 h in medium containing 20% FBS or were exposed to 7-KC 20 μM for 16 h. SMCs were stained with a senescence-associated GLB1 Staining Kit (Cell Biolabs Inc., CBA-230) according to the manufaturer's instructions. The blue stained senescent cells were counted using a light microscope.

Cell proliferation assay

To evaluate the growth response of cultured SMCs to 20% FBS, the BrdU incorporation assay was performed using a cell proliferation kit (Roche Diagnostics, 11647229001) according to the manufacturer's instructions. Briefly, SMCs were plated

at a density of 3,000 cells/well in 96-well culture plates with complete medium. At 60% to 70% confluence, the SMCs were stimulated with 20% FBS for 24 h. Then, BrdU solution (10 μM) was added to the cells and the cells were cultured for a further 4 h. Next, the cells were dried and fixed, and the cellular DNA was denatured with FixDenat solution (Roche Diagnostics, 11647229001) for 30 min at room temperature. A rat anti-BrdU monoclonal antibody conjugated with peroxidase (Roche Diagnostics, 11647229001) was added to the culture plates and incubated again at room temperature for 90 min. Finally, tetramethylbenzidine was added before incubation for 15 min at room temperature. Absorbance at 370 nm was measured using a microplate reader.

Statistical analysis

Differences between 2 groups were examined for statistical significance using the Mann-Whitney t test. Comparisons of more than 3 groups were conducted by one-way analysis of variance followed by the Scheffé method as the post-hoc test. The cumulative event-free rates were estimated from Kaplan Meier survival curves and differences were tested by the log-rank test. *P* values less than 0.05 were considered to indicate a statistically significant difference between 2 groups. Results are expressed as the mean ± SEM. Data were analyzed using the Statistical Package for Social Science computer software program, version 18 (SPSS Inc., Chicago, IL, USA).

Abbreviations

ACTA2	actin, alpha 2, smooth muscle, aorta
APOE	apolipoprotein E
BBC3	BCL2 binding component 3
BP	blood pressure
BrdU	bromodeoxyuridine
CASP3	caspase 3
CCL2	chemokine (C-C motif) ligand 2
ELISA	enzyme-linked immunosorbent assay
FBS	fetal bovine serum
GLB1	galactosidase, beta 1
H2AFX	H2A histone family, member X
7-KC	7-ketocholesterol
LGALS3	lectin, galactose binding, soluble 3
MAP1LC3B	microtubule-associated protein 1 light chain 3 beta
MMP9	matrix metallopeptidase 9
NAC	N-acetylcysteine
PCNA	proliferating cell nuclear antigen
SMCs	smooth muscle cells
SQSTM1	sequestosome 1
TEM	transmission electron microscopy
TAGLN	transgelin
TRP53/TP53	transformation related protein 53

Acknowledgments

We thank Dr. Masaaki Komatsu (Niigata University Graduate School of Medical and Dental Sciences) for providing *Atg7*$^{f/f}$ mice, and Ms. N. Daimaru, Ms. E. Magoshi, Ms. H. Hibino, and Ms. S. Ishikawa for their excellent technical assistance.

Disclosure statement

No potential conflict of interest was reported by the authors.

Funding

This work was supported by grants from the Ministry of Education, Sports and Culture of Japan (to H.W. [JSPS KAKENHI; grant numbers JP 16H01205 and JP 26293220] and (to T.M. [JSPS KAKENHI grant numbers JP 24790782 and JP 16K01833]), and Japan Agency for Medical Research and Development (AMED) (toY.F.[JP18gm0610005]), and the Takeda Science Foundation (to T.M.), Research Fund of Mitsukoshi Health and Welfare foundation 2016 (to T.M.), the Juntendo University Young Investigator Joint Project Award 2015 (grant no. (2710) (to Y.O.), Suzuken Memorial Foundation 2015 (to Y.O.), and MSD Life Science Foundation 2017 (to Y.O.), Japan Foundation for Applied Enzymology (to T.M.), MSD, Ono Pharmaceutical Company, Mitsubishi Tanabe Pharma Corporation, Kowa Company Ltd., and Boehringer Ingelheim Pharmaceuticals, Inc. (to H. W.)

ORCID

Masato Koike http://orcid.org/0000-0002-3174-5684

References

[1] Klionsky DJ. Autophagy: from phenomenology to molecular understanding in less than a decade. Nat Rev Mol Cell Biol. 2007 Nov;8(11):931–937. PubMed PMID: 17712358.
[2] Komatsu M, Waguri S, Chiba T, et al. Loss of autophagy in the central nervous system causes neurodegeneration in mice. Nature. 2006 Jun 15;441(7095):880–884. PubMed PMID: 16625205.
[3] Lin L, Baehrecke EH. Autophagy, cell death, and cancer. Mol Cell Oncol. 2015 Jul-Sep;2(3):e985913. PubMed PMID: 27308466; PubMed Central PMCID: PMC4905302.
[4] Nakai A, Yamaguchi O, Takeda T, et al. The role of autophagy in cardiomyocytes in the basal state and in response to hemodynamic stress. Nat Med. 2007 May;13(5):619–624. PubMed PMID: 17450150.
[5] Ebato C, Uchida T, Arakawa M, et al. Autophagy is important in islet homeostasis and compensatory increase of beta cell mass in response to high-fat diet. Cell Metab. 2008 Oct;8(4):325–332. PubMed PMID: 18840363.
[6] Jones SA, Mills KH, Harris J. Autophagy and inflammatory diseases. Immunol Cell Biol. 2013 Mar;91(3):250–258. PubMed PMID: 23318657.
[7] Ross R. Atherosclerosis–an inflammatory disease. N Engl J Med. 1999 Jan 14;340(2):115–126. PubMed PMID: 9887164.
[8] Lutgens E, de Muinck ED, Kitslaar PJ, et al. Biphasic pattern of cell turnover characterizes the progression from fatty streaks to ruptured human atherosclerotic plaques. Cardiovasc Res. 1999 Feb;41(2):473–479. PubMed PMID: 10341847.
[9] Clarke MC, Figg N, Maguire JJ, et al. Apoptosis of vascular smooth muscle cells induces features of plaque vulnerability in atherosclerosis. Nat Med. 2006 Sep;12(9):1075–1080. PubMed PMID: 16892061.
[10] Clarke MC, Littlewood TD, Figg N, et al. Chronic apoptosis of vascular smooth muscle cells accelerates atherosclerosis and promotes calcification and medial degeneration. Circ Res. 2008 Jun 20;102(12):1529–1538. PubMed PMID: 18497329.
[11] Henderson EL, Geng YJ, Sukhova GK, et al. Death of smooth muscle cells and expression of mediators of apoptosis by T lymphocytes in human abdominal aortic aneurysms. Circulation. 1999 Jan 5- 12;99(1):96–104. PubMed PMID: 9884385.
[12] Salabei JK, Hill BG. Implications of autophagy for vascular smooth muscle cell function and plasticity. Free Radic Biol Med. 2013 Dec;65:693–703. PubMed PMID: 23938401; PubMed Central PMCID: PMC3859773.
[13] Martinet W, De Meyer GR. Autophagy in atherosclerosis: a cell survival and death phenomenon with therapeutic potential. Circ Res. 2009 Feb 13;104(3):304–317. PubMed PMID: 19213965.
[14] Hill BG, Haberzettl P, Ahmed Y, et al. Unsaturated lipid peroxidation-derived aldehydes activate autophagy in vascular smooth-

muscle cells. Biochem J. 2008 Mar 15;410(3):525–534. PubMed PMID: 18052926.
[15] Chen YC, Bui AV, Diesch J, et al. A novel mouse model of atherosclerotic plaque instability for drug testing and mechanistic/therapeutic discoveries using gene and microRNA expression profiling. Circ Res. 2013 Jul 19;113(3):252–265. PubMed PMID: 23748430.
[16] Xu K, Yang Y, Yan M, et al. Autophagy plays a protective role in free cholesterol overload-induced death of smooth muscle cells. J Lipid Res. 2010 Sep;51(9):2581–2590. PubMed PMID: 20484746; PubMed Central PMCID: PMC2918441.
[17] Michiels CF, Fransen P, De Munck DG, et al. Defective autophagy in vascular smooth muscle cells alters contractility and Ca2+ homeostasis in mice. Am J Physiol Heart Circ Physiol. 2015 Mar 15;308(6):H557–67. PubMed PMID: 25576626.
[18] Grootaert MO, da Costa Martins PA, Bitsch N, et al. Defective autophagy in vascular smooth muscle cells accelerates senescence and promotes neointima formation and atherogenesis. Autophagy. 2015 Nov 02;11(11):2014–2032. PubMed PMID: 26391655; PubMed Central PMCID: PMC4824610.
[19] Holtwick R, Gotthardt M, Skryabin B, et al. Smooth muscle-selective deletion of guanylyl cyclase-A prevents the acute but not chronic effects of ANP on blood pressure. Proc Natl Acad Sci USA. 2002 May 14;99(10):7142–7147. PubMed PMID: 11997476; PubMed Central PMCID: PMC124542.
[20] Mizushima N, Yoshimori T, Levine B. Methods in mammalian autophagy research. Cell. 2010 Feb 5;140(3):313–326. PubMed PMID: 20144757; PubMed Central PMCID: PMC2852113.
[21] Madamanchi NR, Vendrov A, Runge MS. Oxidative stress and vascular disease. Arterioscler Thromb Vasc Biol. 2005 Jan;25 (1):29–38. PubMed PMID: 15539615.
[22] Kuivaniemi H, Ryer EJ, Elmore JR, et al. Update on abdominal aortic aneurysm research: from clinical to genetic studies. Scientifica. 2014;2014:564734. PubMed PMID: 24834361; PubMed Central PMCID: PMC4009235.
[23] Sandberg EM, Sayeski PP. Jak2 tyrosine kinase mediates oxidative stress-induced apoptosis in vascular smooth muscle cells. J Biol Chem. 2004 Aug 13;279(33):34547–34552. PubMed PMID: 15159394.
[24] Clowes AW, Clowes MM, Reidy MA. Kinetics of cellular proliferation after arterial injury. III. Endothelial and smooth muscle growth in chronically denuded vessels. Lab Invest. 1986 Mar;54 (3):295–303. PubMed PMID: 3512908.
[25] Saraff K, Babamusta F, Cassis LA, et al. Aortic dissection precedes formation of aneurysms and atherosclerosis in angiotensin II-infused, apolipoprotein E-deficient mice. Arterioscler Thromb Vasc Biol. 2003 Sep 1;23(9):1621–1626. PubMed PMID: 12855482.
[26] Finn AV, Nakano M, Narula J, et al. Concept of vulnerable/unstable plaque. Arterioscler Thromb Vasc Biol. 2010 Jul;30 (7):1282–1292. PubMed PMID: 20554950.
[27] Bennett MR, Sinha S, Owens GK. Vascular Smooth Muscle Cells in Atherosclerosis. Circ Res. 2016 Feb 19;118(4):692–702. PubMed PMID: 26892967; PubMed Central PMCID: PMC4762053.
[28] Razani B, Feng C, Coleman T, et al. Autophagy links inflammasomes to atherosclerotic progression. Cell Metab. 2012 Apr 04;15 (4):534–544. PubMed PMID: 22440612; PubMed Central PMCID: PMC3322320.
[29] Ward MR, Pasterkamp G, Yeung AC, et al. Arterial remodeling - Mechanisms and clinical implications. Circulation. 2000 Sep 5;102 (10):1186–1191. PubMed PMID: WOS:000089157400020; English.
[30] Yamanouchi D, Morgan S, Kato K, et al. Effects of caspase inhibitor on angiotensin II-induced abdominal aortic aneurysm in apolipoprotein E-deficient mice. Arterioscler Thromb Vasc Biol. 2010 Apr;30(4):702–707. PubMed PMID: 20075419.
[31] Sakalihasan N, Limet R, Defawe OD. Abdominal aortic aneurysm. Lancet. 2005 Apr 30;365(9470):1577–1589. PubMed PMID: WOS:000228754800030; English.
[32] Lu H, Aikawa M. Many faces of matrix metalloproteinases in aortic aneurysms. Arterioscler Thromb Vasc Biol. 2015 Apr;35 (4):752–754. PubMed PMID: 25810296.
[33] Howatt DA, Dajee M, Xie X, et al. Relaxin and matrix metalloproteinase-9 in Angiotensin II-Induced abdominal aortic aneurysms. Circ J. 2017 May 25;81(6):888–890. PubMed PMID: 28420827.
[34] Salio M, Puleston DJ, Mathan TS, et al. Essential role for autophagy during invariant NKT cell development. Proc Natl Acad Sci USA. 2014 Dec 30;111(52):E5678–87. PubMed PMID: 25512546; PubMed Central PMCID: PMC4284579.
[35] Schaub FJ, Han DK, Liles WC, et al. Fas/FADD-mediated activation of a specific program of inflammatory gene expression in vascular smooth muscle cells. Nat Med. 2000 Jul;6(7):790–796. PubMed PMID: 10888928.
[36] Lu H, Howatt DA, Balakrishnan A, et al. Subcutaneous angiotensin II Infusion using osmotic pumps induces aortic aneurysms in mice. JoVE. 2015 Sep;28(103). PubMed PMID: 26436287; PubMed Central PMCID: PMC4692630. DOI:10.3791/53191
[37] Komatsu M, Waguri S, Ueno T, et al. Impairment of starvation-induced and constitutive autophagy in Atg7-deficient mice. J Cell Biol. 2005 May 9;169(3):425–434. PubMed PMID: 15866887; PubMed Central PMCID: PMC2171928.
[38] Subramanian V, Golledge J, Ijaz T, et al. Pioglitazone-induced reductions in atherosclerosis occur via smooth muscle cell-specific interaction with PPAR{gamma}. Circ Res. 2010 Oct 15;107(8):953–958. PubMed PMID: 20798360; PubMed Central PMCID: PMC2963621.
[39] Nomiyama T, Nakamachi T, Gizard F, et al. The NR4A orphan nuclear receptor NOR1 is induced by platelet-derived growth factor and mediates vascular smooth muscle cell proliferation. J Biol Chem. 2006 Nov 3;281(44):33467–33476. PubMed PMID: 16945922.
[40] Arakawa M, Mita T, Azuma K, et al. Inhibition of monocyte adhesion to endothelial cells and attenuation of atherosclerotic lesion by a glucagon-like peptide-1 receptor agonist, exendin-4. Diabetes. 2010 Apr;59(4):1030–1037. JST.JSTAGE/endocrj/52.683 [pii]. PubMed PMID: 16410659; eng.
[41] Mita T, Otsuka A, Azuma K, et al. Swings in blood glucose levels accelerate atherogenesis in apolipoprotein E-deficient mice. Biochem Biophys Res Commun. 2007 Jul 6;358(3):679–685. PubMed PMID: 17506980.
[42] Mita T, Goto H, Azuma K, et al. Impact of insulin resistance on enhanced monocyte adhesion to endothelial cells and atherosclerogenesis independent of LDL cholesterol level. Biochem Biophys Res Commun. 2010 May 14;395(4):477–483. S0006-291X(07)00820-0 [pii]10.1016/j.bbrc.2007.04.118. PubMed PMID: 17506980; eng.
[43] Tanida I, Mizushima N, Kiyooka M, et al. Apg7p/Cvt2p: A novel protein-activating enzyme essential for autophagy. Mol Biol Cell. 1999 May;10(5):1367–1379. PubMed PMID: 10233150; PubMed Central PMCID: PMC25280.